



Original article

Innovative deep learning and quantum entropy techniques for brain tumor MRI image edge detection and classification model

Ahmed Alamri ^a, S. Abdel-Khalek ^b, Adel A. Bahaddad ^c , Ahmed Mohammed Alghamdi ^{d,*}^a Department of Information Systems and Technology, College of Computer Science and Engineering, University of Jeddah, Jeddah 21493, Saudi Arabia^b Department of Mathematics and Statistics, College of Science, Taif University, P. O. Box 11099, Taif 21944, Saudi Arabia^c Department of Information System, Faculty of Computing and Information Technology, King Abdulaziz University, Jeddah 21589, Saudi Arabia^d Department of Software Engineering, College of Computer Science and Engineering, University of Jeddah, Jeddah 21493, Saudi Arabia

ARTICLE INFO

ABSTRACT

Keywords:

Brain tumor
Edge detection
Segmentation
Quantum entropy
Multi-image
MRI
Siberian tiger optimization

Brain Tumors (BT) are the foremost basis of cancer death. They are affected by the uncontrolled and abnormal growth of cells in the spinal canal or brain. The main issue with a BT is identifying its shape, location, and dimension. Despite numerous efforts and promising outcomes in tumour recognition, precise classification from benign to malignant type is still difficult. A frequently employed device in analyzing these conditions is a magnetic resource image (MRI); however, medical specialists' physical assessment of MRI images causes troubles owing to time restraints and variability. In the preceding few years, because of artificial intelligence (AI) and deep learning (DL), significant developments have been prepared in medical science, such as the Medical Image processing model, which aids doctors in analyzing disease timely and effortlessly; before that, it was time-consuming and tiresome. This study proposes an Innovative Deep Learning and Quantum Entropy Techniques for Brain Tumor Edge Detection and Classification (IDLQET-BTEDC) model in MRI imaging. The primary goal of the IDLQET-BTEDC model is to improve accuracy and efficiency in identifying BTs using multi-images such as detected and edge images. To accomplish this, the IDLQET-BTEDC approach involves pre-processing, which contains two processes: the wiener filter for noise removal and adaptive gamma correction for contrast enhancement. Furthermore, the segmentation process adopts dual approaches focusing on region and edge detections. The tumour region is segmented using enhanced UNet with NAdam optimization, while the quantum entropy (QE) edge detection is applied to delineate the tumour boundaries. In addition, the IDLQET-BTEDC model performs feature extraction by using Multi-head Attention fusion to combine EfficientNetV2 and Swin transformer (ST). The graph convolutional recurrent neural network (GCRNN) classifier is utilized for BT detection and classification. Finally, the hyperparameter tuning of the GCRNN model is performed by employing the Siberian tiger optimization (STO) model to achieve superior accuracy. To demonstrate the good classification outcome of the IDLQET-BTEDC approach, an extensive range of simulations is performed under the Figshare BT dataset. The performance validation of the IDLQET-BTEDC technique portrayed a superior accuracy value of 98.00 % over existing methods.

1. Introduction

A BT is a group of abnormal cells arising in the brain. It can occur in some individuals at nearly any stage. It could even be modified from one treatment session to the subsequent one, but it is not similar for every individual [1]. BT performs in diverse image strengths at any position and can have various sizes and shapes. BT might be malignant or benign. Benign BT has a similar structure and does not comprise tumour cells [2]. They might be both surgically annihilated and monitored

radiologically, and they rarely increase again. Malignant BT has a diverse structure and comprises tumour cells. In this method, a method that can classify tumours and give more precise outcomes is applied [3]. Tumours might be handled by chemotherapy, radiotherapy, or a mixture of them, and they are life-threatening. Consequently, analyzing the BT in a proper period is highly required for further treatments. MRI is mainly utilized and prevalent for BT analysis compared to computerized tomography (CT) scans and other methods [4]. MRI has been verified to be a versatile and powerful brain imaging modality that permits

* Corresponding author.

E-mail address: amalghamdi@uj.edu.sa (A.M. Alghamdi).

Input: Training Images (<https://www.kaggle.com/datasets/ashkhagan/figshare-brain-tumor-dataset>)

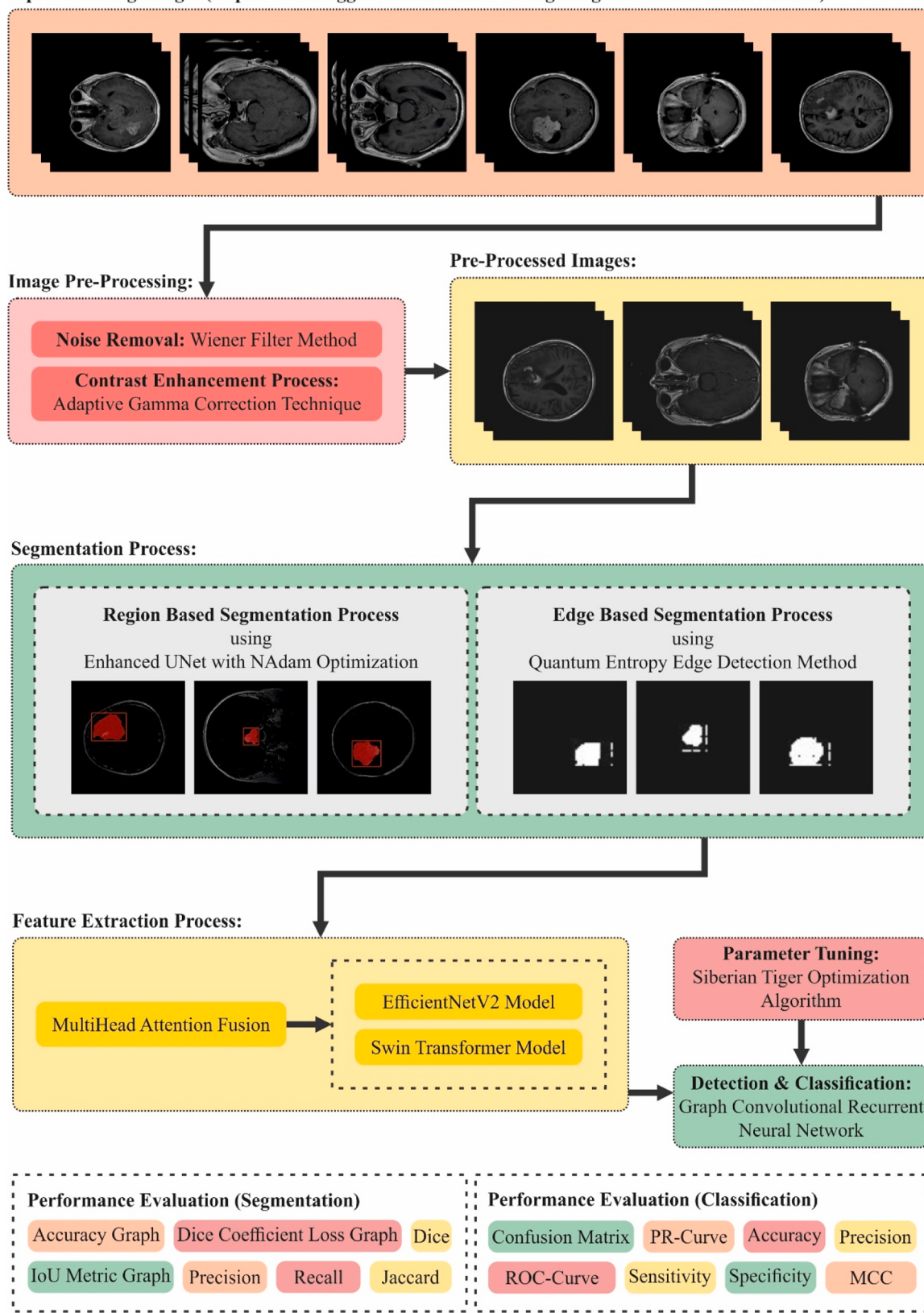


Fig. 1. Overall process of IDLQET-BTEDC approach.

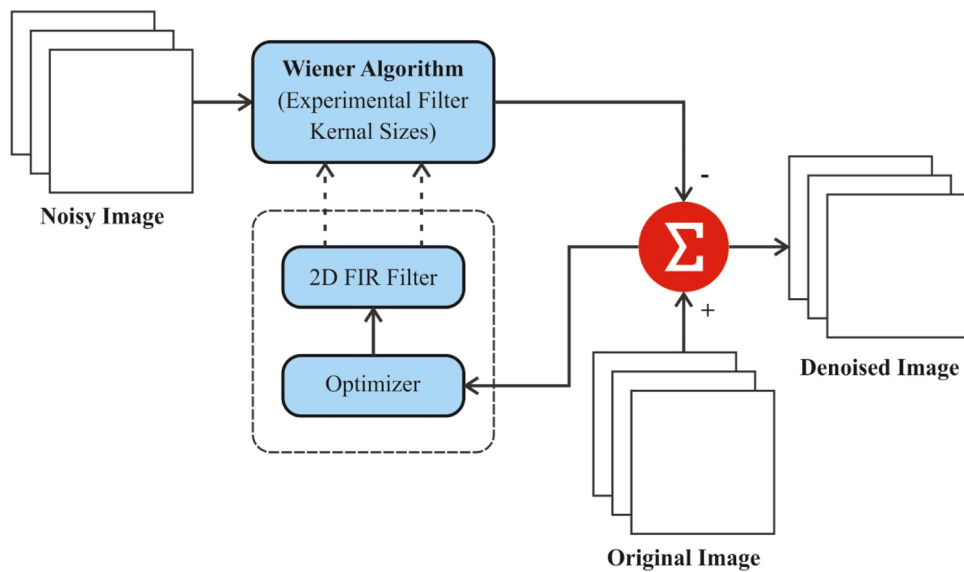


Fig. 2. Structure of the WF model.

non-invasive longitudinal imaging. The MRI information enhances understanding of normal and diseased anatomy for clinical experiments and is a major factor in analysis and treatment planning [5]. MRI is to select the approach for earlier recognition of BT in the human brain. MRI is more advanced, and waves utilize MRI to attain higher-quality images around the tissues and body, allowing MRI to identify the most minor parts of the body. MRI is generally used to treat BT or other cancers [6].

Through high-resolution imaging, MRI, anatomical data, and the discovery of abnormalities, it is concluded that This method has a higher capacity to identify alterations in structures and tissue, which is greater than CT for recognizing the BT size. Human examination is The traditional approach in treating brain MRI classification and cancer recognition [7]. MRI also comprises a noise initiated by operator performance that can cause severe imprecision classification. Usually, MRI data is a vast and complex cognitive process. In recent times, investigators have challenged a difficult concern when it comes to manually segmenting MRI brain images. BT and their positions should be categorized precisely utilizing a classification method [8]. Precise MRI data analysis is not a simple task and is always time-consuming. Many DL and machine learning (ML) methodologies for recognizing BT have been presented in recent decades. Most of those recommended DL and ML methods are aimed at dual BT identification [9]. The convolutional neural network (CNN) is a DL-based method for classifying BT. Benign and Malignant tumour classification is gained from this approach [10]. A deep neural network-based 3D-CNN is employed for BT segmentation.

This study proposes an Innovative Deep Learning and Quantum Entropy Techniques for Brain Tumor Edge Detection and Classification (IDLQET-BTEDC) model in MRI imaging. The primary goal of the IDLQET-BTEDC model is to improve accuracy and efficiency in identifying BTs using multi-images such as detected and edge images. To accomplish this, the IDLQET-BTEDC approach involves pre-processing, which contains two processes: the wiener filter for noise removal and adaptive gamma correction for contrast enhancement. Furthermore, the segmentation process adopts dual approaches focusing on region and edge detections. The tumour region is segmented using enhanced UNet with NAdam optimization, while the quantum entropy (QE) edge

detection is applied to delineate the tumour boundaries. In addition, the IDLQET-BTEDC model performs feature extraction by using Multi-head Attention fusion to combine EfficientNetV2 and Swin transformer (ST). The graph convolutional recurrent neural network (GCRNN) classifier is utilized for BT detection and classification. Finally, the hyperparameter tuning of the GCRNN model is performed by employing the Siberian tiger optimization (STO) model to achieve superior accuracy. To demonstrate the good classification outcome of the IDLQET-BTEDC approach, an extensive range of simulations is performed under the Figshare BT dataset. The key contribution of the IDLQET-BTEDC approach is listed below.

- The IDLQET-BTEDC model improves input data quality by applying a WF for effectual noise removal and adaptive gamma correction for contrast enhancement. This pre-processing step ensures more precise and detailed images, enhancing subsequent tumour detection accuracy. These techniques assist the overall performance by mitigating distortions and enhancing key features in the data.
- The tumour region is accurately segmented by utilizing an enhanced UNet model optimized with NAdam, enhancing the tumour delineation's precision. This method allows for better feature extraction, resulting in more reliable segmentation results. Using NAdam optimization improves the model's capability to adapt to complex data, improving overall performance.
- The IDLQET-BTEDC technique implements QE edge detection to delineate the tumour boundaries, improving segmentation accuracy precisely. This methodology enhances the detection of boundary features by utilizing quantum-based techniques. As a result, it assists in achieving more reliable and accurate tumour localization in medical images.
- The IDLQET-BTEDC method efficiently tunes the GCRNN classifier with the STO model, enhancing the accuracy and robustness of BT detection. The incorporation of these techniques enables improved feature extraction and classification performance. This approach ensures a more reliable and precise detection of BTs from medical imaging data.

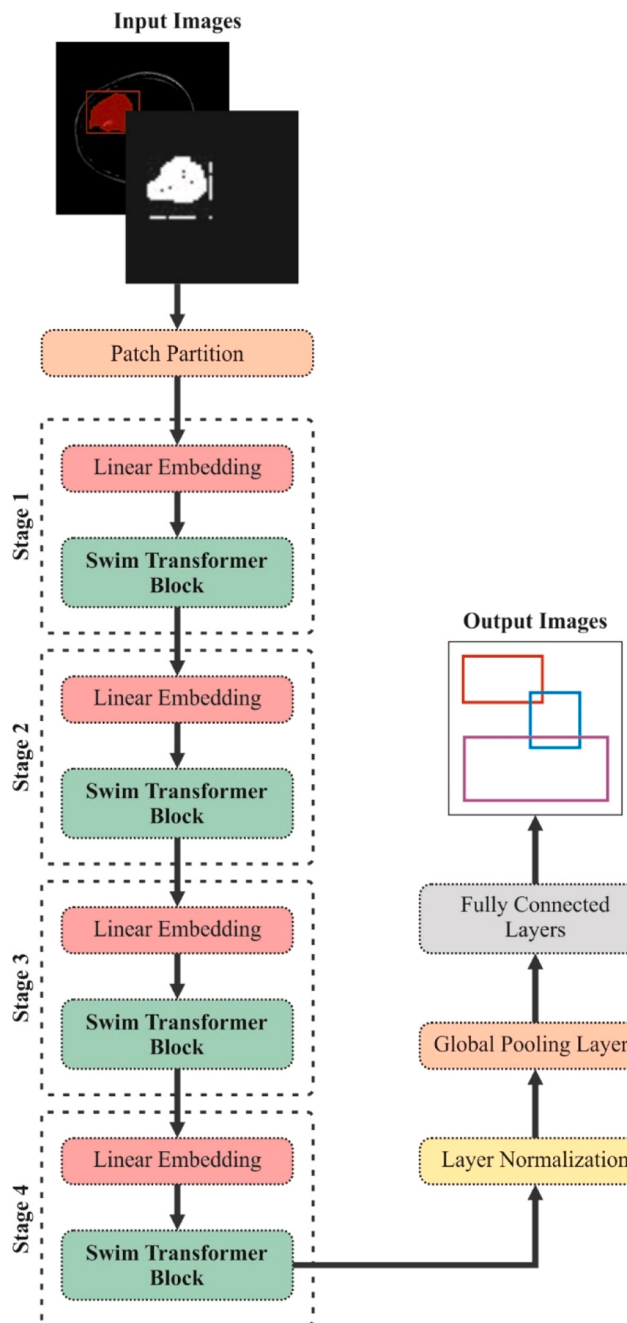


Fig. 3. Architecture of Swim Transformer.

- The novelty of the IDLQET-BTEDC methodology is integrating Multi-head Attention fusion with EfficientNetV2 and ST for feature extraction. This incorporation improves the technique's capability to capture intrinsic features from medical images, enhancing classification accuracy. The model attains greater robustness and performance in BT detection by utilizing advanced DL techniques.

2. Review of literature

Vu and Vajda [11] project a new method which associates edge recognition with a hierarchical DL structure. By employing a dual-phase method, primarily segregating pituitary and meta-tumor class and then filtering the meta-tumor class into meningioma and glioma with a dual classifier, this work exploits the capacities of both developed neural network (NN) and classical image processing. The resNet50 structure

has already been demonstrated, and the backbone method is advantageous from Transfer Learning (TL). Allah et al. [12] proposed a DCNN, called the Edge U-Net method, formed as an encoding-decoding framework stimulated by the U-Net structure. The Edge U-Net method can more accurately localize cancers by combining boundary-related MRI information. In the decoder phase, boundary-related data from diverse scales of original MRIs can be incorporated with the proper adjacent contextual data. Hameed et al. [13] projected an innovative method by demonstrating three improved DL methods, namely ResNet50, EfficientNetB6, and EfficientNetBO, on MRI dataset examples, depicting each one of 4 diversities of BT. Developed NN structures implemented this investigation. This method also applies TL methods to enhance its performance. In [14], a BT segmentation approach depends on deep semantic fusions, and edge information in a multimodal MRI image is projected. This approach primarily contains feature fusion, edge detection, and semantic segmentation components. The ST is implemented for extraction in the segmentation part. Asiri et al. [15] developed a new, two-module computerized approach focused on raising the accuracy and speed of BT recognition. The Image Enhancement method employs 3 ML and imaging approaches, independent component analysis, adaptive Wiener filtering, and NN, to standardize images and combat concerns like noise and changing lower region dissimilarity. The second module utilizes SVM to validate the first module output and accomplish tumour classification and segmentation. Prathipati and Satpathy [16] present a new method employing fragmentation. The projected Multilevel De-noising method with Precision Edge-based Fragmentation for Tumor Size Diagnosis (MD-PES-TSD) has been projected as a complete structure for the segmentation and detection of MRI imaging. Kanagamalliga and Rajappiahdarshine [17] proposed a new pre-processing method tailored to improve the skull area in MRI image visibility, helping in the accurate BT detection and segmentation of the tumour area. Utilizing CNN for segmentation and classification through thresholding, the approach addresses the difficulties caused by the wider skull area in the coronal and sagittal plane brain MRI images. The recommended method improves identifying tumour accuracy and reduces computational complexity by integrating developed pre-processing methods. In [18], multi-layer CNN structures are presented. It presents two significant investigations to assess the performance and accuracy of the system. Initially, a five-layer CNN structure with five layers and two diverse split ratios. Then, a six-layer CNN structure with two diverse split ratios.

Rajamohana et al. [19] present a novel approach incorporating classical and hybrid quantum-inspired graph neural networks for tumour classification. Classical Graph CNNs (GCNN) analyze complex relationships within medical imaging data, while hybrid Quantum Graph Neural Networks (QGNN) enhance performance by utilizing principles of quantum computing. Ullah et al. [20] introduce a DL method for brain tumour classification. Pretrained networks are optimized, and features are integrated using a Quantum Theory-based Marine Predator Optimization algorithm (QTbMPA) for final classification. Bilal et al. [21] present a hybrid model integrating an Extreme Learning Machine (ELM) with FuNet TL using the Quantum-Genetic Binary Grey Wolf Optimizer (Q-GBGWO) technique. This method utilizes a diverse feature fusion strategy, improving the extraction of critical imaging features, while Q-GBGWO optimizes ELM parameters to achieve superior classification performance. Albalawi et al. [22] introduce a novel CNN architecture designed to enhance the accuracy and efficiency of brain tumour detection in MRI scans. This method focused on multi-task classification by utilizing a single CNN technique for various brain MRI classification tasks, comprising tumour detection, classification based on grade and type, and tumour location identification. Masood, Mzoughi, and Saidani [23] proposed an improved Quantum Theory-based Marine Predator Optimization algorithm (QTbMPA) methodology. The proposed QTbMPA selects both networks' best features and finally fuses utilizing a serial-based approach. The fused feature set is passed to neural network classifiers for the final classification. Abd-Ellah et al. [24] present an automatic brain tumour diagnosis system employing

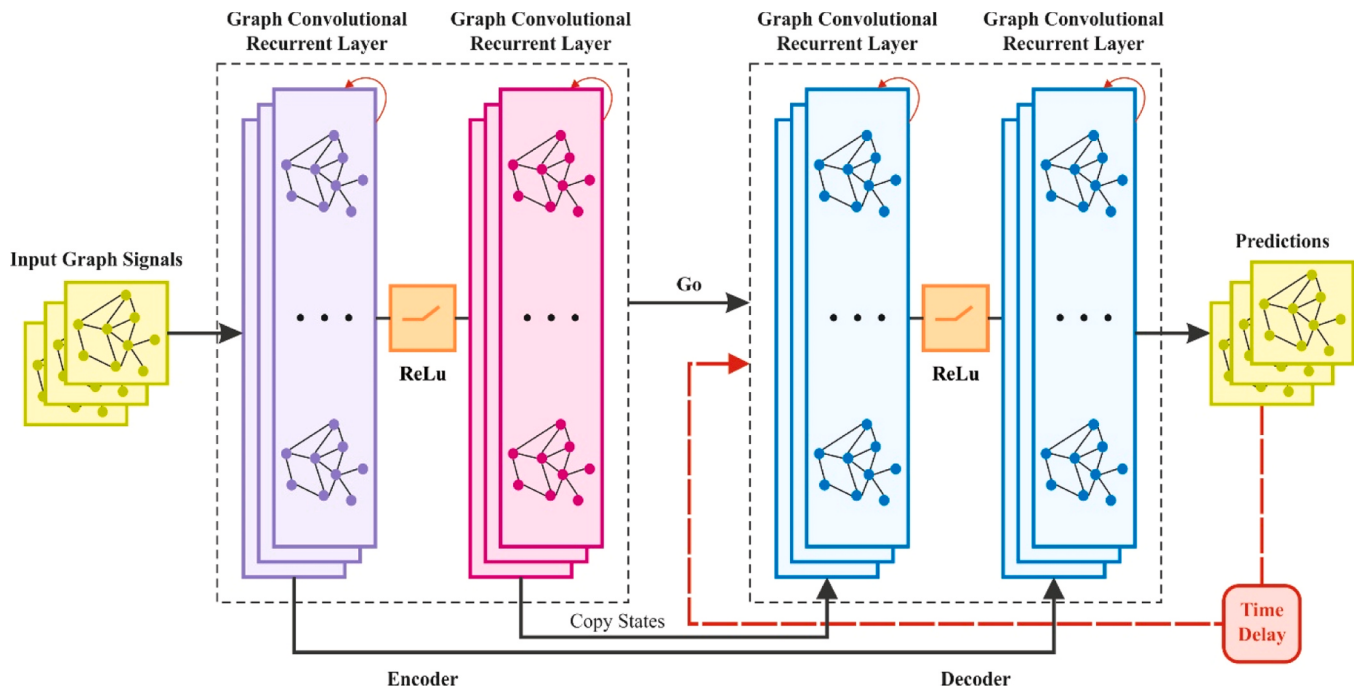


Fig. 4. Structure of the GCRNN method.

CNN to detect, classify, and segment glioblastomas. It comprises two stages: detecting and classifying glioma MRI images and tumour segmentation with skip connections and residual units. Katkam et al. [25] present a multi-class neurodegenerative disease classification using pre-processing techniques. The CapsNet model extracts features, and the Modified DenseNet-169 model performs the classification. Disease regions are then segmented with the Enhanced DeepLabV3+ model. Aamir et al. [26] introduce a hyperparametric CNN model for brain tumour detection, optimizing key hyperparameters to enhance feature extraction, reduce complexity, and enhance diagnostic accuracy. Saeed et al. [27] propose a Dual-Branch Ensemble and Gated Global-Local Attention network based on EfficientNetV2 and ConvNeXt (GGLA-NeXtE2NET) approach to improve accuracy and interpretability. It captures global and local features, handles image variety, and uses ESRGAN for noise reduction in MRI images. Dénes-Fazakas et al. [28] propose L-net, a novel architecture incorporating a U-net for tumour boundary segmentation and a CNN for tumour classification. These two units are coupled so that the CNN classifies the MRI images based on the features extracted by the U-net while segmenting the tumour instead of relying on the original input images.

Despite the improvements in brain tumour detection and segmentation, existing methods still encounter challenges such as handling imbalanced datasets, enhancing accuracy in tumour classification, and mitigating computational complexity. Many approaches depend heavily on pre-trained models, which may not be well generalized to diverse MRI data. Furthermore, issues such as noise in MRI images and difficulty accurately segmenting tumour boundaries remain persistent. While some models integrate hybrid methods, such as quantum-inspired methods and attention mechanisms, their practical implementation is often limited by computational costs and model interpretability. Further research is required to improve these models' robustness, efficiency, and

generalization in real-world clinical settings.

3. Materials and methods

In this study, the IDLQET-BTEDC model in MRI images is proposed. The primary goal of the IDLQET-BTEDC model is to improve accuracy and efficiency in identifying BT using multi-images such as detected and edge images. To accomplish this, the IDLQET-BTEDC model has pre-processing contains two processes, namely noise removal and contrast enhancement; segmentation adopts dual approaches focusing on both region detection using enhanced UNet with NAdam optimization, and QE edge detection, multi-head attention fusion to combine EfficientNetV2 and ST, GCRNN based BT detection, and STO based parameter tuning. Fig. 1 demonstrates the entire process of the IDLQET-BTEDC methodology.

3.1. Pre-processing

Initially, the IDLQET-BTEDC approach involves pre-processing, which contains two processes: the WF for noise removal and adaptive gamma correction for contrast enhancement.

3.1.1. Noise removal: WF

The WF is an influential model for removing noise, mainly beneficial in medical image processing, like BT recognition in MRI images [29]. This model is chosen due to its capability to adapt to varying noise levels across an image, giving an effectual solution for medical imaging applications where noise can be unpredictable. Unlike conventional filters, WF considers the local mean and variance of the image, ensuring improved preservation of crucial image features while removing noise. This adaptability assists in retaining the quality of critical structures in

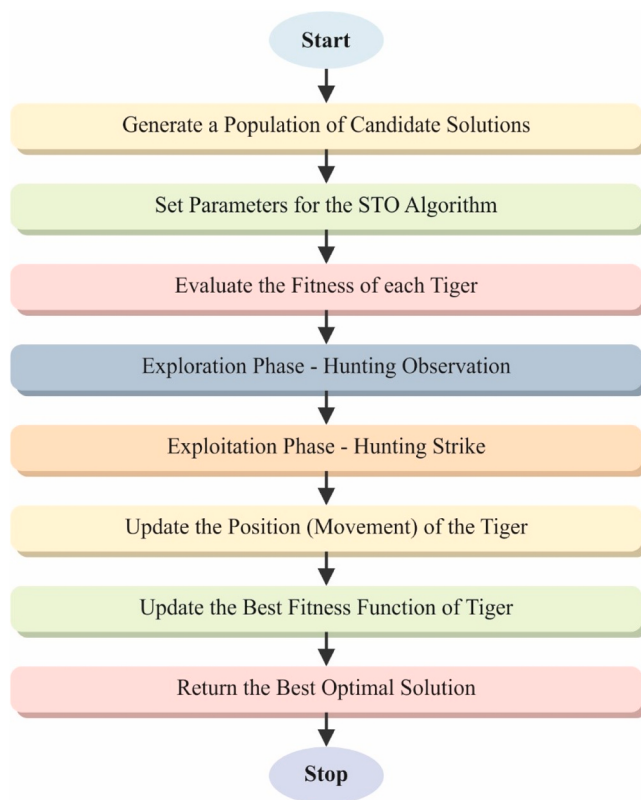


Fig. 5. Architecture of the STO methodology.

medical images, such as tumour boundaries, which is significant for accurate analysis. Moreover, WF performs well even in low signal-to-noise ratio scenarios, making it ideal for MRI or CT scans where image clarity can be compromised. Furthermore, WF optimizes the trade-off between noise reduction and edge preservation compared to other techniques like Gaussian or median filters. This makes it an ideal choice for pre-processing in BT detection. Fig. 2 illustrates the WF framework.

It minimizes the mean square error between the desired and noisy images, efficiently flattening out noise while maintaining significant image details. Recognition of BTs aids in removing artefacts and noise from MRI scans, enhancing the simplicity of critical features such as tumour boundaries. Using the WF, image processing stages such as classification and segmentation can function more effectively to improve tumour recognition accuracy. This noise reduction system is particularly advantageous for MRI scans, where noise can unclear fine details, making it problematic to differentiate tumour areas from good tissue.

3.1.2. Contrast enhancement: adaptive gamma correction

Adaptive gamma correction is a method employed to alter the contrast and brightness of images by using a non-linear transformation depending upon the image's intensity spreading [30]. This model is chosen as it effectually adjusts the brightness and contrast of an image based on local image characteristics, ensuring that both dark and bright areas are improved without overexposing essential details. Unlike conventional methods, AGC dynamically adapts to the local content of the image, making it more appropriate for medical images where contrast

variations can crucially affect the visibility of critical features, such as tumour regions. This adaptability is valuable for brain tumour detection, where subtle differences in tissue density must be emphasized. Additionally, AGC performs superiorly in improving low-contrast areas, making it more efficient than global contrast adjustment methods. By preserving the overall structure of the image while enhancing local contrast, AGC improves the visibility of tumours, resulting in improved segmentation and classification outcomes. This flexibility and precision make AGC more reliable than other contrast enhancement methods, especially in cases with low contrast or noisy images. Furthermore, its capability to maintain important image features while improving tumor areas ensures more accurate and consistent results across various MRI datasets.

This technique is adaptive naturally, altering the gamma value locally for dissimilar areas in the image to improve facts without underexposing or overexposing parts of the image. Its mathematical formulation is formulated below:

$$I_{\text{output}}(x,y) = \left(\frac{I_{\text{input}}(x,y)}{L_{\max}} \right)^{\gamma(x,y)} \cdot L_{\max} \quad (1)$$

$I_{\text{output}}(x,y)$ and $I_{\text{input}}(x,y)$ denote a modified and original pixel intensity at positions (x,y) , respectively. L_{\max} indicates a maximum intensity value. $\gamma(x,y)$ represents an adaptive gamma value computed depending on local image features.

3.2. Segmentation process

Following, the segmentation procedure adopts dual approaches focusing on both region and edge detections. The tumour region is segmented using enhanced UNet with NAdam optimization, while the QE edge detection is applied to delineate the tumour boundaries. This model is chosen because it can capture fine-grained details and spatial hierarchies in medical images. UNet's encoder-decoder architecture is specifically effectual for biomedical image segmentation, where precise localization of tumour regions is significant. The NAdam optimizer, which incorporates the merits of both Adam and Nesterov momentum, improves convergence speed and accuracy during training, making the model more robust and efficient than other optimizers. Furthermore, QE edge detection is applied to precisely delineate tumour boundaries, enhancing segmentation accuracy by capturing high-contrast edges with minimal noise. This integration of UNet and QE edge detection utilizes the capability of the DL method to segment complex structures while addressing challenges like image noise and poor contrast, which may affect conventional segmentation methods. Together, they provide an optimal balance of accuracy, robustness, and computational efficiency.

3.2.1. Region-based segmentation

The encoder region of the Unet network mainly contains dual 3×3 convolution layers characterized by light blue, the layer of max-pooling of dimensions 2×2 symbolized by light gray, and the decoder region contains 2×2 up sampling signified by light gray and 2×2 convolution layers denoted by light green in inverted convolution layer and dual 3×3 convolution layers symbolized by light blue. Each convolution utilizes the Rectified Linear Unit (*ReLU*) as an activation function [31]. Unet+ separates the encoding and decoding portions of the novel Unet network into sub-modules, comprising an encoder and a decoder. During the encoding, all sub-modules downsample the input image two times successively and remove features utilizing a convolution layer; within the decoder, every sub-module up samples and fuses the previous

Table 1
Details of Dataset.

Class	No. of Images
Glioma	1426
Meningioma	708
Pituitary	930
Total Images	3064

output level using the encoding features, followed by implementing the decoder process at the following level. Finally, the Unet++ output is designed by integrating the outputs of each sub-module.

Here, the Gaussian Error Linear Unit (*GeLU*) has been presented as the activation function in an enhanced Unet network. Even though the *GeLU* and *ReLU* are extensively applied in the DL domain, the *GeLU* selection for any particular case might improve performance. The novel *GeLU* activation function resolved the problem, which *ReLU* might result in the dispersal of non-positive gradient and rough distribution of data. It presented the function of the Sigmoid based on *ReLU*, which completes its output more efficiently and decreases the oscillation problems within the neural network. The method has superior generalizability and precision to increase the particle segmentation performance. The mathematical formulation is given below:

$$GeLU(x) = 0.5 \times x \left(1 + \tanh \left[\sqrt{\frac{2}{\pi}} (x + 0.0447x^3) \right] \right) \quad (2)$$

This work combined the Squeeze-and-Excitation (SE) attention mechanism (AM) in the Unet system, which mainly improved the

attention of the models to significant features by dynamically regulating the weightings of all channels within the input feature mapping. This mechanism initially compressed an input feature mapping into a vector utilizing the global average pooling process, followed by learning a weighted vector over dual fully connected (FC) layers comprising all channels' weighted information. At last, this weighted vector has been multiplied by the new input feature mapping to gain the improved feature mapping. During this Unet network, the SE-AM is applied to improve the attention in reconstruction and feature extraction. In this work, the residual mechanism has been presented to enhance the double *conv* portion of the Unet network, and every convolution layer is accompanied by *GeLU* and normalization layers (BatchNorm-2d) to improve the feature learning capability, and SE-AM has been included in the Unet network.

Nadam is an optimizer model introduced for effective stochastic optimization that demands a first-order gradient using low memory requirements [32]. This model is easier to execute, computationally effective, and contains small memory needs. Nevertheless, it doesn't change for diagonal gradient scaling and is appropriate for larger difficulties by parameter or data. Nadam applied Nesterov's accelerated gradient (NAG) and retained the momentum of the Adams module as a benefit. It created a replacement, which improved the convergence speed and the quality of the models. Nadam is one of the stochastic gradient descents. This model tasks in DL to upgrade the weight and bias values to decrease the resultant loss. The Nadam model in Eq. (3) was utilized in the backpropagation (BP) method to upgrade the bias and weight on the parameter w_{t+1} , while t denotes the time step, and w_t refers to the present weight. L means loss function value, whereas the

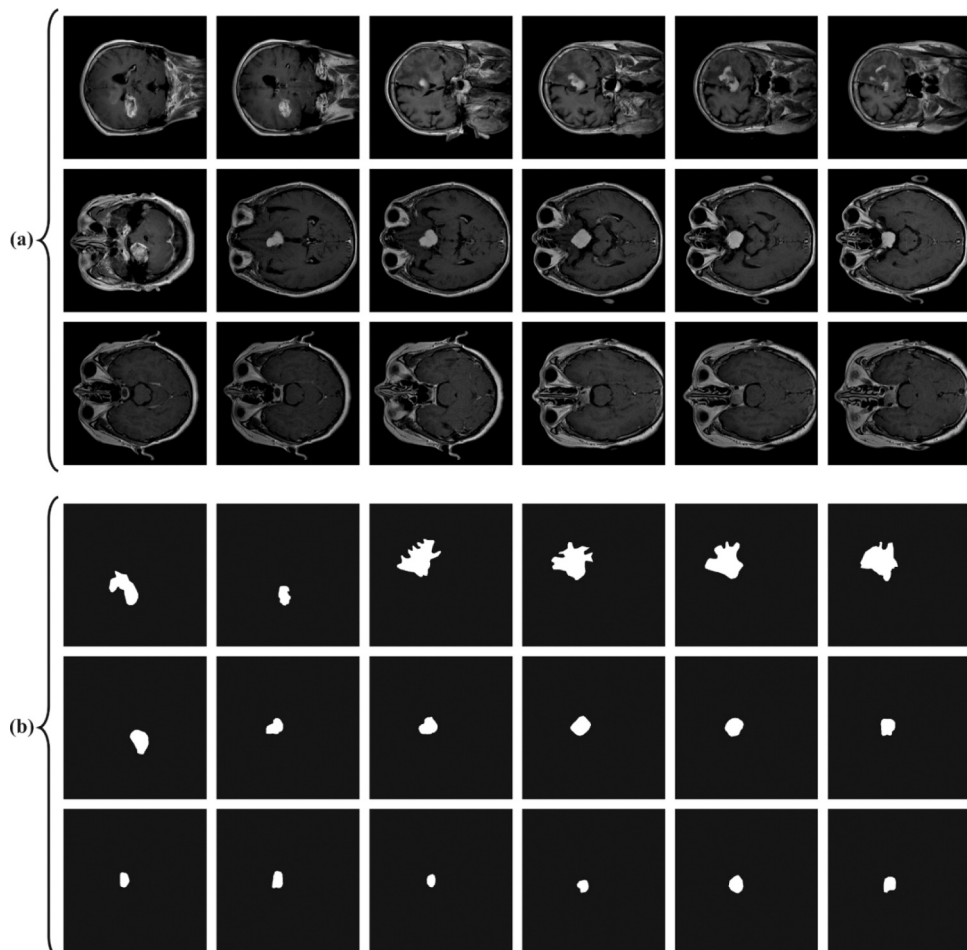


Fig. 6. Sample of (a) original image (b) masked image.

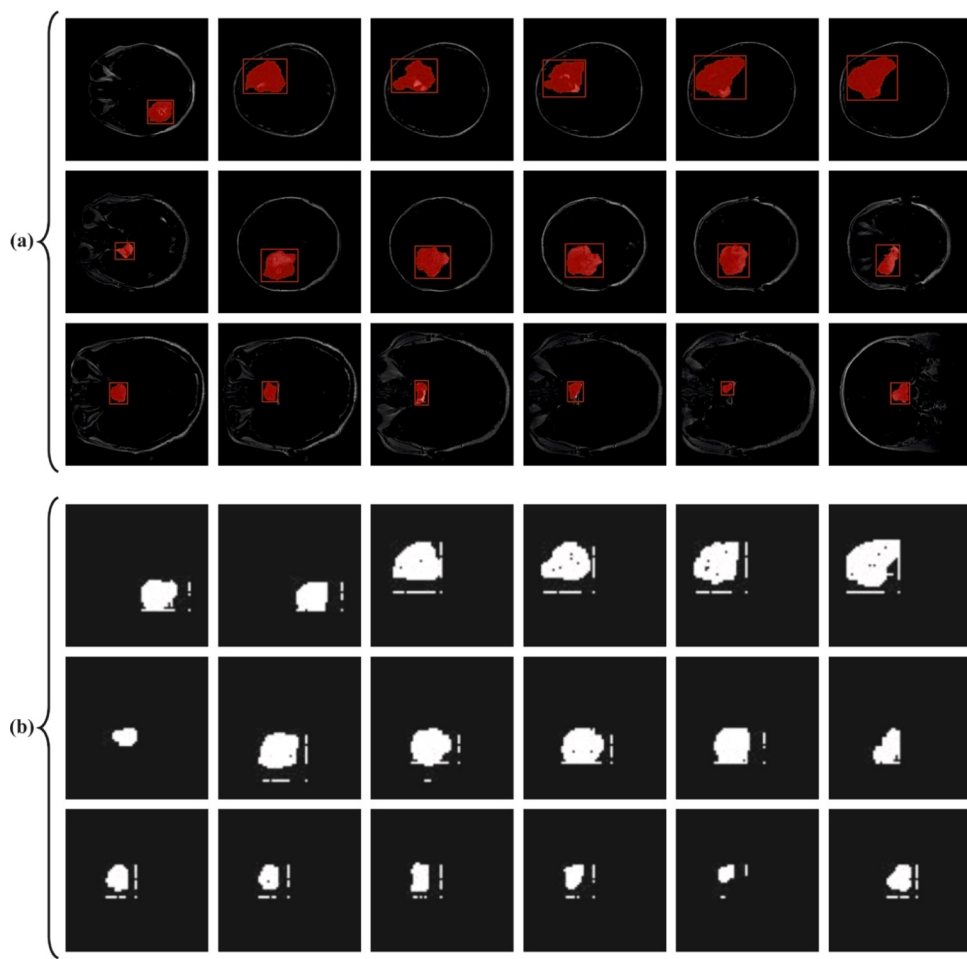


Fig. 7. Sample of (a) segmented image (b) edge image.

Table 2
Segmented Results of IDLQET-BTEDC method under TRAST and TESST.

Metrics	Training Set	Testing Set
Prec _n	91.71	92.00
Rec _a	86.24	86.33
Dice	88.89	89.08
Jaccard	80.00	80.30

learning rate parameter values α and decay β are modifiable as required. Moreover, the average exponential movement of gradient V and square gradient S was started using zero.

$$w_{t+1} = w_t - \frac{a}{\sqrt{s + \epsilon}} \left(\beta_1 \hat{V}_t + \frac{1 - \beta_1}{1 - \beta_1^t} \cdot \delta L \right) \quad (3)$$

Nadam optimization was selected because it is more effective and efficient and does not apply several resources.

3.2.2. Edge-based segmentation

QE is considered the expansion of Shannon entropy (SE) [33]. SE calculates the variable's data amount, and QE calculates the ambiguity of a quantum condition.

Given quantum information systems (QIS) $|\varphi\rangle\}$ which holds states of N $|\varphi_1\rangle, |\varphi_2\rangle, \dots, |\varphi_N\rangle$, at that N states follow the probabilities $|p_1\rangle, |p_2\rangle, \dots, |p_N\rangle$, this QIS is stated as shown:

$$\begin{cases} |\varphi_1\rangle, |\varphi_2\rangle, \dots, |\varphi_N\rangle, \\ |p_1\rangle, |p_2\rangle, \dots, |p_N\rangle, \end{cases} \quad (4)$$

The density matrix (operator) of this QIS states

$$\rho = \sum_{i=1}^N P_i |\varphi_i\rangle \langle \varphi_i| \quad (5)$$

The von Neumann entropy or QE for a QIS $|\phi\rangle$ is described as

$$S(\rho) \equiv -\text{tr}(\rho \log \rho) \quad (6)$$

Whereas $|\rangle$ denotes Dirac ket notation, ρ signifies the densities matrix of the quantum condition, $|\varphi\rangle$, and $0 \log 0 \equiv 0$ if $\rho = 0$.

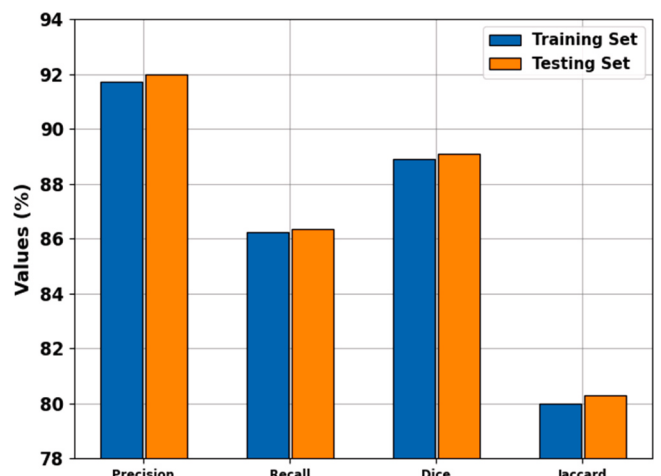


Fig. 8. Average of IDLQET-BTEDC method under TRAST and TESST.

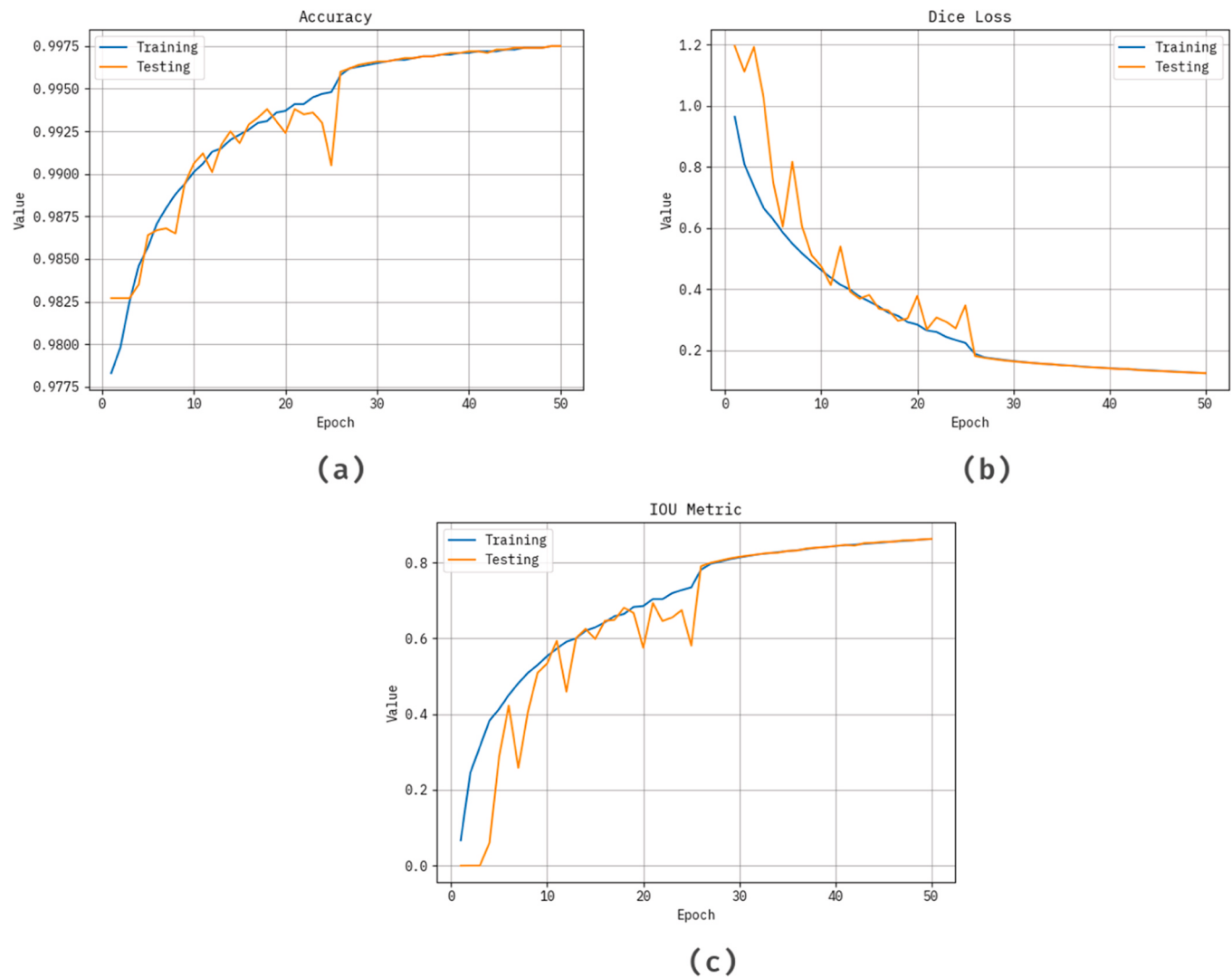


Fig. 9. Result analysis for segmented graph a) Accuracy b) Dice Loss c) IOU Metric.

Table 3
Comparative analysis of IDLQET-BTEDC model with existing techniques.

Method	Dice Score	Prec _n	Recal _t
IDLQET-BTEDC	89.08	92.00	86.33
MI	65.27	72.26	77.25
HOG	70.27	76.27	82.30
SURF	74.28	79.27	84.27
DeepMedic	82.07	90.07	74.05
BTS-HCNN	88.06	90.07	84.06
CycleGAN	74.07	79.07	84.08
IIB-DRN Model	85.07	88.07	83.08

QE can determine the non-local connection among quantum methods or amongst quantum foundations; it is more precise than the SE in the dimensions of quantum information. The quasi-threshold, which results in maximal QE, must be accepted as the optimum threshold since the maximum amount of information is gained in such a case. QE of the digital image might take association property amongst pixels included, whereas the SE is weak,

$$H(X) = H(p_1, p_2, \dots, p_N) = - \sum_{j=1}^N p_j \log p_j \quad (7)$$

Whereas p_1, p_2, \dots, p_N are probabilities of the variable values X . The SE is equivalent to the von Neumann entropy when p_1, p_2, \dots, p_N are consid-

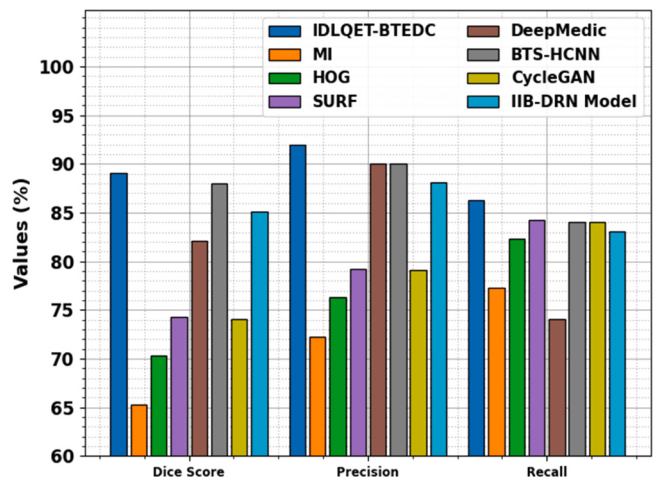


Fig. 10. Comparative analysis of IDLQET-BTEDC model with existing techniques.

ered density matrix eigenvalues. After the conditions are non-orthogonal, the von Neumann entropies calculate the shortcoming of the equivalent quantum condition, but the resource of the shortcoming

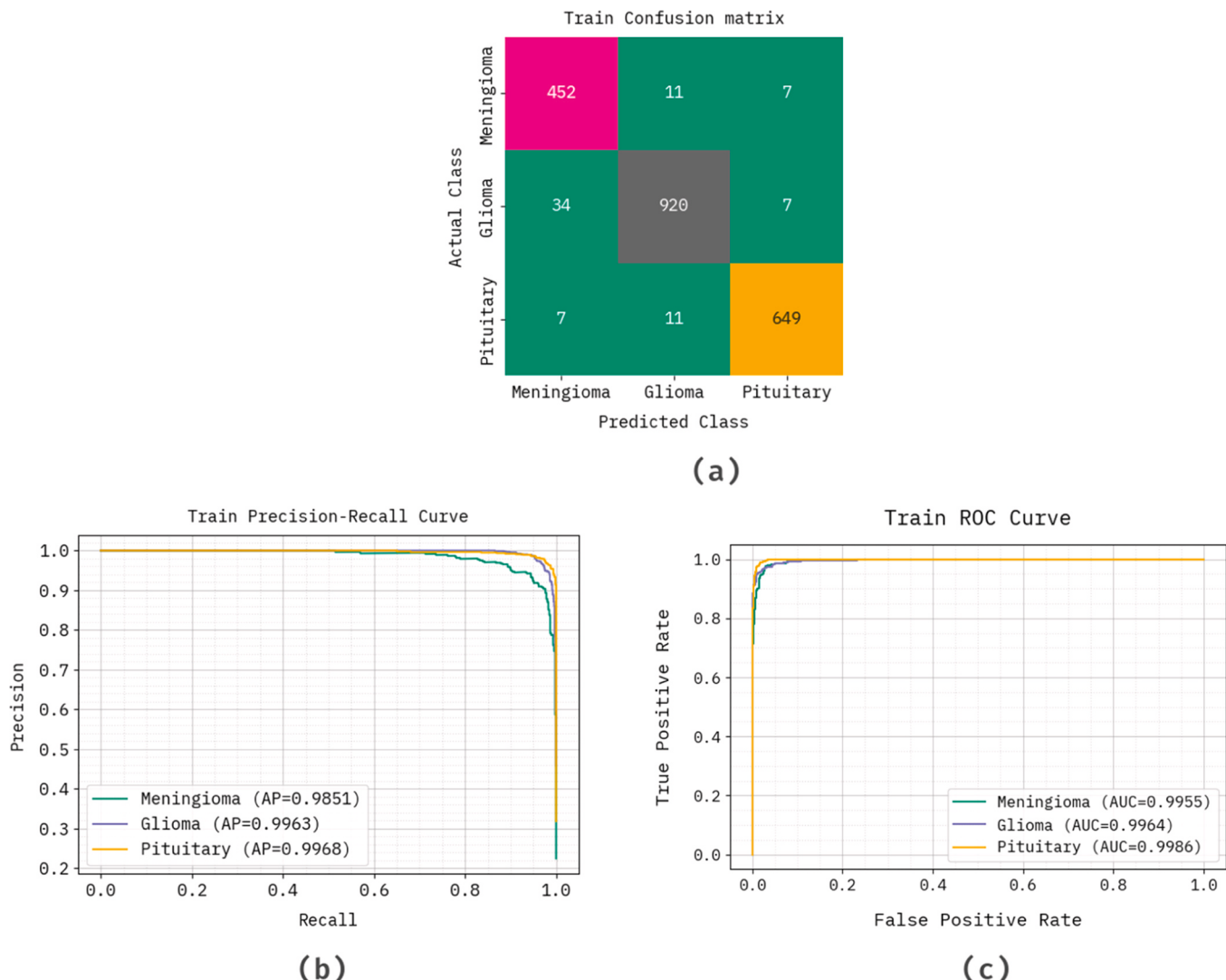


Fig. 11. Results analysis for TRAST a) confusion matrix b) Curve of PR c) Curve of ROC.

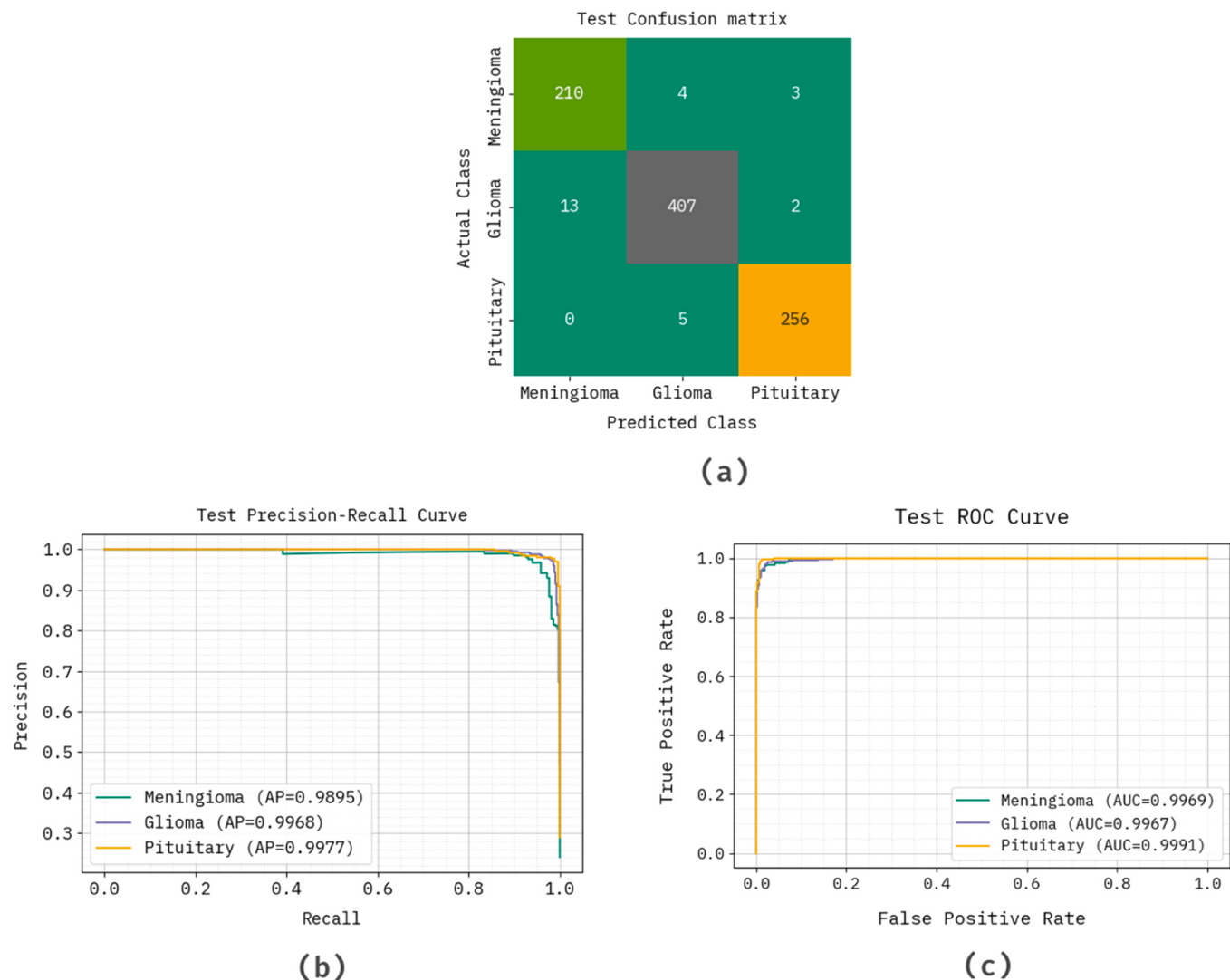


Fig. 12. Results analysis for TESST a) confusion matrix b) Curve of PR c) Curve of ROC.

Table 4
TRAST and TESST outcome of IDLQET-BTEDC method under dissimilar metrics.

Metrics	Training Set	Testing Set
$Accu_y$	97.55	98.00
$Prec_n$	95.75	96.70
$Recall$	96.40	97.10
$F1_{score}$	96.05	96.89
MCC	94.18	95.32

rests unidentified. Therefore, when correlations between pixels are considered as the cross-correlations of elementary conditions in quantum methods, the QE of the digital image can capture correlation assets amongst pixels included, whereas the SE is weak. Therefore, this is the conceptual basis of the model presented. Integrating quantum mechanics enhances edge detection's precision, especially in complex medical images like brain MRIs.

3.3. Fusion of feature extraction

In addition, the IDLQET-BTEDC model performs feature extraction using Multi-head Attention fusion to combine EfficientNetV2 and ST. This model presents crucial advantages over conventional methods. EfficientNetV2 has a highly effective architecture, achieving superior

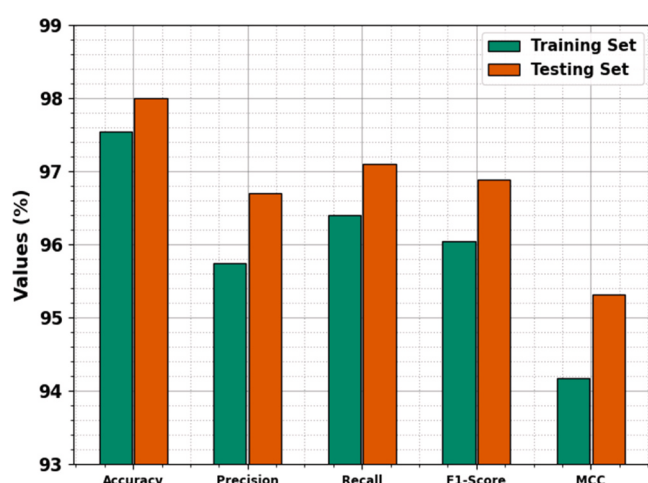


Fig. 13. TRAST and TESST outcome of IDLQET-BTEDC method under dissimilar metrics.

Table 5

Comparison analysis of the IDLQET-BTEDC methodology with existing models [39–45].

Framework	<i>Accu_y</i>	<i>Prec_n</i>	<i>Recal_t</i>	<i>F1_{score}</i>
Novel 2D-CNN	97.05	95.45	95.81	92.70
Novel 3D-CNN	89.57	93.07	96.88	95.41
VGG-19 Classifier	90.76	95.98	94.01	92.37
Inception-V3 Model	95.67	92.91	92.64	95.75
Fine-tuned VGG-19	94.06	93.77	96.40	93.18
3D-CNN Method	97.37	95.06	96.12	95.03
YOLOv5m	90.33	93.62	96.52	95.95
GAN	91.29	96.04	94.78	92.95
BERT	96.31	93.70	93.31	96.08
IDLQET-BTEDC	98.00	96.70	97.10	96.89

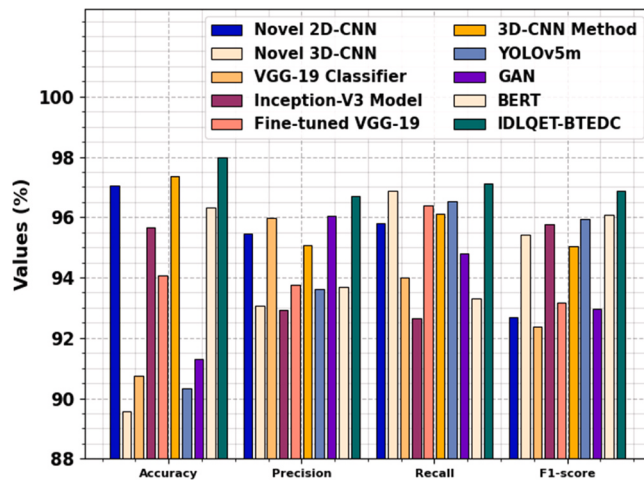


Fig. 14. Comparison analysis of IDLQET-BTEDC methodology with existing models.

performance with fewer parameters and lower computational cost, making it ideal for handling complex medical imaging tasks. The ST, on the contrary, captures long-range dependencies and local context through its hierarchical structure, which improves feature extraction in diverse spatial regions. By applying Multi-head Attention, the model can concentrate on diverse features at various scales, enhancing its capability for extracting critical information from the input data. This integration of EfficientNetV2 and ST employs the strengths of both convolutional and transformer-based models, enabling the extraction of more meaningful and discriminative features. Compared to conventional feature extraction methods, this approach presents enhanced accuracy and robustness, particularly in complex image classification tasks, where capturing fine-grained and global context is crucial.

3.3.1. EfficientNetV2

The CNN must utilize a brief structure with fewer parameters to enhance performance and minimize overfittings, like the VGG method or EfficientNetV2 [34]. The backbone of CNN has progressed in this study and is stimulated by EfficientNetV2. Then, the CNN branch was intended to depend upon EfficientNetV2, providing promising outcomes. EfficientNetV2 acts as a CNN subdivision of Eff-Swin, mainly concentrating on removing shallow features and repeatedly enhancing them to take local features. To improve accuracy, this paper presents the channel attention (CA) mechanism to improve EfficientNetV2. This improvement increases the learning of vital positional data. EfficientNetV2 generally contains 3 initial methods: *S*, *M*, and *L*. The simplest method, EfficientNetV2-S, has been selected as the development's foundation for minimizing overfitting and attaining optimum performance. Even though EfficientNetV2-S is very simple and easy amongst the initial

Table 6

PT outcome of IDLQET-BTEDC technique with existing models.

Framework	PT (sec)
Novel 2D-CNN	6.50
Novel 3D-CNN	3.40
VGG-19 Classifier	6.83
Inception-V3 Model	7.19
Fine-tuned VGG-19	3.45
3D-CNN Method	3.78
YOLOv5m	5.09
GAN	6.11
BERT	7.09
IDLQET-BTEDC	2.31

methods delivered by an original author, it meets tasks throughout training, with higher computation demands, long training periods, and the main typical space occupation. To tackle these problems, an original network structure layer has been improved.

Set the lesser development proportion of MBConv against Fused-MBConv outcomes in lesser memory access above. Fused-MBConv is utilized only in early dual phases. On the other hand, MBConv modules were employed in the last 4 phases to enhance the method's lightweight features. Besides, the SE module is substituted for both modules with a CA. Then, 5x5 convolutional kernels through an original 3x3 kernel in the MBConv are used to improve accuracy and decrease the number of convolution layers. Next, these main a reduced necessity for a convolutional layer to endure accuracy declining the system layers in phases 1 over 6–1, 2, 2, 3, 4, and 4 layers, correspondingly. By utilizing some convolutional layers other than EfficientNetV2, this structure mainly improves the extraction of feature ability.

3.3.2. ST

The ST is the finest in global modelling, thus accurately seizing global dependencies. Therefore, for upholding spatial data efficiently, the ST branch has been presented to complement the extraction of the feature procedure. The ST is a graphic technique that mainly depends upon the Transformer structure, which improves the generalizability and applicability of Transformers over models like hierarchical structure, block-wise self-attention, and multi-scale fusion. This hierarchical architecture permits ST to alter various tasks. In the preliminary phase, a 224x224x3 image is input into the patch divider and separated into manifold non-overlapping patches of dimension 4x4, where each patch holds sizes of 4x4x3. In phase 2, the divided patches are input into a linear layer of embedding for converting the dimension of the feature to C and next served into a block of ST. It acts as a self-attention computa-

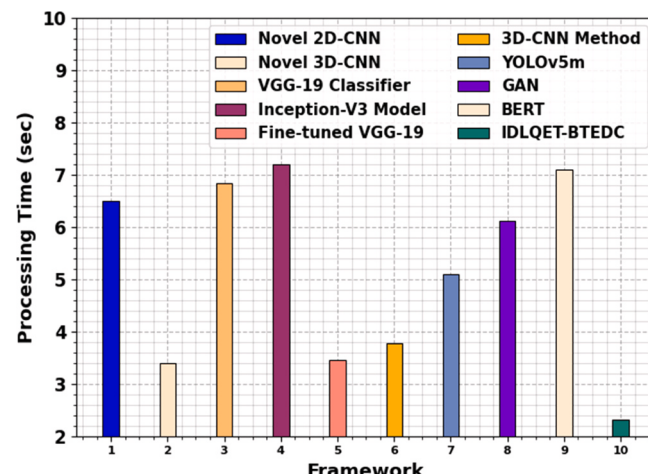


Fig. 15. PT outcome of IDLQET-BTEDC technique with existing models.

tation to remove the feature of the image, and the subsequent output has been delivered to the following phase. The procedure includes patch uniting for Phases 2–4, where input from the preceding phase is united into 2x2 dimensions for combining nearby windows. Then, these compound feature maps are an input to produce a hierarchical representation of the feature. Throughout this procedure, the patch uniting layer manages dimensionality upsurge and downsampling while the block of ST removes image features. Fig. 3 represents the structure of the swim transformer.

3.3.3. Fusion of multi-head attention

The multi-head AM is presented, which employs scaled dot product attention [35]. It calculates the dot product of the query by each of the keys, split by $\sqrt{D_k}$, and utilizes the softmax function to gain the weightings on the values. The consistent expression is exposed in Eq. (8). D_k denotes column counts of the metrics K and Q , for example, the dimension of the vectors. The query (Q) characterizes the data that the method is required to hunt for; the key (K) denotes the index applied to recover data, and the value (V) represents real data itself. The significance of value is verified by computing the similarities between key and query. Additionally, the weighting amount of significant values has been applied to get the last output of the method. The equation was exposed in Eq. (9); $X = [x_1, x_2, x_3, \dots, x_n]$ characterizes input data, and W_q, W_k, W_v symbolizes weight matrices gained during the training.

$$\text{Attention}(Q, K, V) = \text{softmax}\left(\frac{QK^T}{\sqrt{D_k}}\right)V \quad (8)$$

$$Q = W_q X$$

$$K = W_k X \quad (9)$$

$$V = W_v X$$

During this mechanism, every collection of segmented input parameters is estimated in various subdivisions of the higher dimension area. Attention weights are next calculated in all subdivisions utilizing the scaled dot-product attention that individually assigns attention to input attributes in all subspaces. Finally, the outputs of all subspaces are connected cooperatively to make the last outputs. This model improves the algorithm's capability to concentrate on input data and enables implementation. W^0, W_i^Q, W_i^K , and W_i^V represent parameter matrices for the linear transformation.

$$\text{MultiHead}(Q, K, V) = \text{Concat}(\text{head}_1, \dots, \text{head}_h)W^0$$

$$\text{head}_i = \text{Attention}(QW_i^Q, KW_i^K, VW_i^V) \quad (10)$$

Meanwhile, attention is distributed in various subspaces. Multi-head attention searches for relations amongst various viewpoints of input information, encrypting many nuances and relations. Numerous autonomous heads of the multi-head attention method can concentrate on dissimilar data together, either global or local, to remove more complete and enhanced features. This integration enhances feature representation, enabling precise and robust performance in tasks like segmentation and classification.

3.4. BT detection employing GCRNN method

For the BT recognition and classification process, the GCRNN classifier is utilized [36]. This model is chosen due to its ability to model spatial and temporal dependencies simultaneously. GCRNN integrates the merits of GCN, which effectively captures relationships between pixels or regions in an image, and RNN, which outperforms at capturing temporal dependencies in sequential data. This hybrid architecture allows for a more comprehensive analysis of tumour regions, both spatially and temporally. Compared to conventional CNN or RNN-based

models, GCRNN can better model the complex spatial relationships and dynamic changes across diverse brain layers, enhancing classification accuracy. The model's capacity to handle graph-structured data, where each pixel or region is treated as a node, enables more precise detection of tumour boundaries and classification. This approach improves the performance and robustness of the model, giving significant enhancements over conventional methods that face difficulty with complex interdependencies between regions in BR images. Fig. 4 depicts the GCRNN architecture.

The convolution operation is extensively applied for ML and data-driven model growth, and it is mainly described as a weight-sharing process between neighbouring regions in space or time to calculate several transformations and operations. Regarding DL, a traditional CNN utilizes convolutional operations on the (multi-dimensional) arrays, which hold spatial meanings. CNNs are generally applied for classification goals like image recognition; then, images are observed as matrices within the Euclidean space. CNNs have shown effective performance in visual analytics and signal handling because of their natural ability to address this type of structure, removing meaningful characteristics, which are divided using the data and applied to various studies. Common graph CNN (GCNs) can handle graph data by a related area rule besides CNNs; afterwards, a description of appropriate processes and/or data transformation. It is presented to utilize the convolutional process over the GCN structure, which intends to remove nodule features from the graph structures. It is a generality of the convolutional process from grid frameworks, such as an image, to the graph's structure. During this work, the GCN's objective is to give a node representation by utilizing similar nodule features as well as the nodule features of the neighbours. The GCN's output method usually is calculated as shown:

$$Y = \tilde{A}XW \quad (11)$$

Whereas X characterizes the input data, Y refers to the output, but W signifies the matrix using the model parameters. Additionally, \tilde{A} means standardized matrix of adjacency, which is defined as:

$$\tilde{A} = \left(\hat{D}^{-\frac{1}{2}} \hat{A} \hat{D}^{-\frac{1}{2}} \right) \quad (12)$$

By $\hat{A} = A + I$, and while A denotes the matrix of adjacency depending on the graph, whereas the relations characterize the connection between the dissimilar time series, I stands for the matrix of identity, and \hat{D} denotes a matrix of a diagonal degree of \hat{A} . Here, the matrix A is established on the correlation coefficients beside the comprehensive time series of requirements, which means it is continuous over time. As the problem of predicting, the vector X signifies the data, and it is intended to alter constantly in time. Otherwise, matrix A characterizes the connection between nodes so that the convolutional operation can accurately depict the graph. Specifically, the graph's structure keeps on continuous over time as the adjacency matrix is static, whereas the node characteristics change.

Recurrent NNs (RNNs) are specific structures that generate predictions using input data and neighbour unit outputs. The outcome is a network structure using links between neurons, intentionally designed to provide data from the previous. The intelligence of this architecture type exists in the relationship among hidden layers (HL), which are either in time or among layers. In this model, the vector $x = (x_1, \dots, x_t)$ characterizes the input sequences, the vector $y = (y_1, \dots, y_t)$ denotes the output sequence, and $h^n = (h_1^n, \dots, h_t^n)$ characterize the vector sequences within the n -th layer. The common HL h_t of the initial layer is computed in the equation below:

$$h_t^1 = \tanh(W_{xh^1}x_t + W_{hh^1}h_{t-1}^1 + b_h^1) \quad (13)$$

W signifies the weighted matrices, whereas W_{xh^1} refers to the

connection weight between the initial input and the HL. However, $W_{h^{n-1}h^n}$ signifies the weight of a recurrent link in the initial HL, and b_h^1 characterizes the bias. Generally, the HL of the n th layer is considered as shown:

$$h_t^n = \tanh(W_{h^{n-1}h^n}h_t^{n-1} + W_{h^n h^n}h_{t-1}^n + b_h^n) \quad (14)$$

Here, $W_{h^{n-1}h^n}$ characterizes the weight allocated to a link between the n and $n-1$ layers. The weight $W_{h^n h^n}$ signifies the weight assigned to the recurrent link of the n th layer, and b_h^n represents relative bias. The mathematical formulation is expressed below:

$$y_t = W_{h^n y}h_t^n + b_y \quad (15)$$

Now, $W_{h^n y}$ symbolizes weight allocated to the link between the output and n th layer and denotes bias. This type of structure can undergo the problem of gradient vanishing, which means the RNNx0 might have difficulties learning long-period dependence information. Then, various recurrent units, such as the LSTM or the gated recurrent unit (GRU), are presented to solve this problem. This work accepts the LSTM as recurrent units, assuming the similarities among these dual structures. In other words, the equations remain valid, but the HL of all units is computed as shown:

$$f_t = \sigma(W_f h_{t-1}^n + w_f h_t^{n-1} + b_f) \quad (16)$$

$$i_t = \sigma(W_i h_{t-1}^n + w_i h_t^{n-1} + b_i) \quad (17)$$

$$C_t = f_t C_{t-1} + i_t \tanh(W_c h_{t-1}^n + w_c h_t^{n-1} + b_c) \quad (18)$$

$$o_t = \sigma(W_o h_{t-1}^n + w_o h_t^{n-1} + b_o) \quad (19)$$

$$h_t = o_t \tanh(C_t) \quad (20)$$

The accepted activation function for the gates denotes the hyperbolic tangent (tanh) and sigmoid (σ). The conditions of the forget, the input, and the output gate states are correspondingly signified by f_t, i_t, o_t , and C_t . Furthermore, the biases and weights allocated to this gate are $b_o, w_o, W_i, b_c, w_c, W_f, b_f, w_f$ and W_o and b_o, w_o .

The presented RNN's design is one of numerous likelihoods. The RNN collected by LSTM elements was applied to construct the GCRNN and n benchmark methods during this study.

The basic concept of the spatiotemporal GCRNN combines various models of information presented by GCN and the recurrent layer. RNNs are intended to take temporal information, whereas GCNs characterize spatial relationships over a structure of the graph. The mixture of these dual frameworks developed the GCRNN, which is the corresponding integration of these GCNs and RNNs to capture the benefits of their powers in temporal and spatial representation. This method is addressed sequentially by removing the spatial and temporal data from the information. The final dense layer obtains the spatiotemporal model to give the last forecast.

3.5. Parameter optimizer using STO model

Finally, the hyperparameter tuning of the GCRNN model is performed by utilizing the STO approach to achieve superior accuracy [37]. This model is an advanced nature-inspired algorithm based on the behaviour of Siberian tigers, known for their hunting tactics and territorial instincts. Its application as a parameter optimizer is highly effective due to its capability to explore the search space efficiently and avoid

local optima. Compared to conventional optimization algorithms, STO presents a better balance between exploration and exploitation, making it appropriate for fine-tuning DL models with complex parameters. STO's population-based approach allows it to maintain diversity in solutions, enhancing robustness and preventing premature convergence. This is valuable in models with numerous parameters, like those in DL-based brain tumour detection, where finding the global optimal solution is significant. Additionally, STO has shown superior performance in both convergence speed and solution quality, making it an ideal choice for optimizing the parameters in advanced models such as GCRNN for BT detection. Fig. 5 represents the steps involved in the STO technique.

STO is a nature-inspired meta-heuristic optimizer method. It is established to simulate the ST's strategies and behaviours. After searching for prey and fighting bears. During this method, every ST is a component of the complete population and a possible solution. The group of STs is visually represented in matrix format as

$$X = \begin{bmatrix} X_1 \\ \vdots \\ X_i \\ \vdots \\ X_n \end{bmatrix} = \begin{bmatrix} x_{1,1} & \dots & x_{1,i} & \dots & x_{1,m} \\ \vdots & \ddots & \vdots & \ddots & \vdots \\ x_{i,l} & \dots & x_{ii} & \dots & x_{i,m} \\ \vdots & \ddots & \vdots & \ddots & \vdots \\ x_{n,1} & \dots & x_{ni} & \dots & x_{n,m} \end{bmatrix} \quad (21)$$

Where n characterizes the ST counts, and m signifies the variable counts. X_i denotes the i th individual amongst the STs. At the beginning of the STO performance, the first location of STs in the search space is shown as

$$x_{ii} = LB_j + \alpha_{ii} \cdot (UB_j - LB_j) \quad (22)$$

For $i = 1, 2, \dots, n$ and $j = 1, 2, \dots, m$, while x_{ij} signifies the j th size of X_i inside the searching region. Now, α_{ij} characterizes a randomly generated number range between (0-1), whereas LB_i and UB_i designate the lower and upper limits of the j th variable, correspondingly. The target function for every ST is stated as the following vector:

$$\varphi = \begin{bmatrix} \varphi_1 \\ \vdots \\ \varphi_i \\ \vdots \\ \varphi_n \end{bmatrix}_{n \times 1} = \begin{bmatrix} \varphi(X_1) \\ \vdots \\ \varphi(X_i) \\ \vdots \\ \varphi(X_n) \end{bmatrix}_{n \times 1} \quad (23)$$

Here φ , it signifies the objective function vectors, and φ_i characterizes the objective value function for the i th ST. In the first stage of prey pursuing in the design of STO, the potential prey positions for every ST are chosen from the members of the population showing greater values of the objective function, described as shown:

$$P_i = \{X_r | r \in \{1, 2, \dots, n\} \wedge \varphi_r < \varphi_i\} \cup \{X_b\} \quad (24)$$

Here, X_b characterizes the optimum candidate solution. Then, single members (signified as T_i) are arbitrarily chosen from a cluster P_i as the objective in i th ST. The novel location is mathematically expressed in Eq. (25):

$$x_{ij}^{new} = x_{ij} + \alpha_{ij} \cdot (T_{ij} - \beta_{ij} \cdot x_{ij}) \quad (25)$$

Now T_{ij} characterizes the j th size of T_i , and x_{ij}^{new} signifies the j th size of the novel location of the i th member in the 1st stage of STO. The β_{ij} value is either 1 or 2, while i and j are numbers that range between 1 to n and 1 to m , correspondingly. During the next phase, the locations of the population members will be upgraded based on the hunt procedure. This mechanism enhances local exploitation and exploration capability, enabling better solutions. Algorithm 1 demonstrates the STO model.

Algorithm 1. STO Technique

<p>1. Initialization:</p> <ul style="list-style-type: none"> • Randomly initialize a population of tigers (candidate solutions). Each tiger represents a potential solution in the search space. • Set parameters: maximum iterations (<code>max_iter</code>), population size (<code>N</code>), and other algorithm-specific parameters. <p>2. Fitness Evaluation:</p> <ul style="list-style-type: none"> • Evaluate the fitness of each tiger (solution) based on the objective function. <p>3. Territorial Boundaries:</p> <ul style="list-style-type: none"> • Each tiger has a territorial range based on its fitness. Tigers with better fitness are more likely to protect their territory. • Compute the best tiger in the population (the most fit solution). <p>4. Exploration and Exploitation:</p> <ul style="list-style-type: none"> • Exploration: Tigers with lower fitness search the space beyond their territory, mimicking the hunting behaviour. This exploration encourages diversity in the population and prevents premature convergence. • Exploitation: Tigers closer to the best solution (with better fitness) exploit the area around them, increasing the chances of finding the optimal solution. <p>5. Movement Update:</p> <ul style="list-style-type: none"> • Each tiger's position is updated using two components: <ul style="list-style-type: none"> ◦ Exploration Update: Random movements away from the best solution (to explore new regions of the search space). ◦ Exploitation Update: Moves towards the best solution (to fine-tune the current position). • The movement of each tiger is updated using the following formula: <ul style="list-style-type: none"> ◦ $x_i = x_i + \alpha * (X_{best} - x_i)$ where: <ul style="list-style-type: none"> ▪ x_i is the current position of the tiger i, ▪ X_{best} is the position of the best tiger (best solution), ▪ α is the step size or learning rate. <p>6. Territorial Adjustment:</p> <ul style="list-style-type: none"> • If a tiger reaches the territory boundary of a better solution (i.e., it surpasses the best fitness), it adjusts its position to stay within its territory's range. <p>7. Convergence:</p> <ul style="list-style-type: none"> • Repeat the update process for a specified number of iterations (<code>max_iter</code>). • Stop the algorithm if the stopping criteria are met (e.g., maximum fitness or convergence threshold). <p>8. Result:</p> <ul style="list-style-type: none"> • The best solution found during the iterations is returned as the optimal solution.
--

The STO model originates a fitness function (FF) to reach enhanced classification performance. It defines a positive number to indicate the improved efficiency of the candidate solution. In this paper, the minimization of the classifier rate of error is dignified as FF. Its mathematical formulation is shown in Eq. (26).

$$\begin{aligned} \text{fitness}(x_i) &= \text{ClassifierErrorRate}(x_i) \\ &= \frac{\text{no. of misclassified instances}}{\text{Total no. of instances}} \times 100 \end{aligned} \quad (26)$$

4. Experimental validation

In this section, the performance examination of the IDLQET-BTEDC method is verified under the Figshare BT dataset [38]. This dataset covers 3064 images under three class labels, as exposed in Table 1. Fig. 6 signifies the original and masked images sample, and Fig. 7 portrays the segmented and edge images sample.

Table 2 and Fig. 8 represent the segmented results of IDLQET-BTEDC methodology under the training set (TRAST) and testing set (TESST). With TRAST, the IDLQET-BTEDC technique attains prec_n , reca_l , dice , and Jaccard of 91.71 %, 86.24 %, 88.89 %, and 80.00 %, correspondingly. Besides, with TESST, the IDLQET-BTEDC technique attains prec_n , reca_l , dice , and Jaccard of 92.00 %, 86.33 %, 89.08 %, and 80.30 %, respectively.

Fig. 9 illustrates the segmentation outcomes of the IDLQET-BTEDC model. The outcomes specify that the IDLQET-BTEDC model achieves better accuracy, loss of dice, and values of IoU with an increase in epochs. Simultaneously, the IDLQET-BTEDC technique gains decreasing loss values across a rise in epochs.

Table 3 and Fig. 10 depict the comparative analysis of the IDLQET-BTEDC technique with existing methodologies. The values in the table indicate that the IDLQET-BTEDC technique has obtained effectual performance. Based on dice score , the IDLQET-BTEDC approach has higher dice score of 89.08 % while the MI, HOG, SURF, DeepMedic, BTS-HCNN, CycleGAN, and IIB-DRN techniques have lesser dice score of 65.27 %, 70.27 %, 74.28 %, 82.07 %, 88.06 %, 74.07 %, and 85.07 %, respectively.

Besides, dependent on Prec_n , the IDLQET-BTEDC methodology has superior Prec_n of 92.00 % where the MI, HOG, SURF, DeepMedic, BTS-HCNN, CycleGAN, and IIB-DRN approaches have minimal Prec_n of 72.26 %, 76.27 %, 79.27 %, 90.07 %, 90.07 %, 79.07 %, and 88.07 %, correspondingly. Moreover, for Reca_l , the IDLQET-BTEDC methodology has maximal Reca_l of 86.33 % whereas the MI, HOG, SURF, DeepMedic, BTS-HCNN, CycleGAN, and IIB-DRN approaches have minimum Reca_l of 77.25 %, 82.30 %, 84.27 %, 74.05 %, 84.06 %, 84.08 %, and 83.08 %, respectively.

Fig. 11 presents the classifier result of the IDLQET-BTEDC approach under TRAST. Fig. 11a displays the confusion matrix with correct recognition and classification of all classes. Fig. 11b exhibits the PR analysis, representing superior performance over each class label. Simultaneously, Fig. 11c illustrates the ROC curve, signifying capable outcomes with better ROC values for different classes.

Fig. 12 presents the classifier result of the IDLQET-BTEDC methodology under TESST. Fig. 12a illustrates the confusion matrix with perfect identification and classification of every class. Fig. 12b demonstrates the PR curve, indicating maximal performance over all class labels. Fig. 12c shows the ROC analysis, indicating proficient outcomes with high ROC values for dissimilar classes.

Table 4 and Fig. 13 present the TRAST and TESST results of the IDLQET-BTEDC technique under different metrics. With TRAST, the IDLQET-BTEDC model gains u_y , prec_n , reca_l , F1_{score} , and MCC of 97.55 %, 95.75 %, 96.40 %, 96.05 %, and 94.18 %, respectively. Similarly, with TESST, the IDLQET-BTEDC model reaches u_y , prec_n , reca_l , F1_{score} , and MCC of 98.00 %, 96.70 %, 97.10 %, 96.89 %, and 95.32 %, correspondingly.

Table 5 and Fig. 14 portray the comparison analysis of the IDLQET-

BTEDC technique with existing frameworks [39–45]. The table values indicate that the IDLQET-BTEDC technique has obtained effectual performance. Based on acc_y , the IDLQET-BTEDC approach has a higher acc_y of 98.00 %. In contrast, the Novel 2D-CNN, Novel 3D-CNN, VGG-19, Inception-V3, Fine-tuned VGG-19, 3D-CNN, YOLOv5m, Generative Adversarial Networks (GANs), and Bidirectional Encoder Representations from Transformers (BERT) models have lesser acc_y of 97.05 %, 89.57 %, 90.76 %, 95.67 %, 94.06 %, 97.37 %, 90.33 %, 91.29 %, and 96.31 %, respectively. Also, dependent on prec_n , the IDLQET-BTEDC technique has maximum prec_n of 96.70 % where the Novel 2D-CNN, Novel 3D-CNN, VGG-19, Inception-V3, Fine-tuned VGG-19, 3D-CNN, YOLOv5m, GAN, and BERT approaches have lower prec_n of 95.45 %, 93.07 %, 95.98 %, 92.91 %, 93.77 %, 95.06 %, 93.62 %, 96.04 %, and 93.70 %, correspondingly. In addition, for reca_l , the IDLQET-BTEDC technique has a better reca_l of 97.10 %, whereas the Novel 2D-CNN, Novel 3D-CNN, VGG-19, Inception-V3, Fine-tuned VGG-19, 3D-CNN, YOLOv5m, GAN, and BERT methods have inferior reca_l of 95.81 %, 96.88 %, 94.01 %, 92.64 %, 96.40 %, 96.12 %, 96.52 %, 94.78 %, and 93.31 %, respectively. At last, based on F1_{score} , the IDLQET-BTEDC model has maximal F1_{score} of 96.89 % while the Novel 2D-CNN, Novel 3D-CNN, VGG-19, Inception-V3, Fine-tuned VGG-19, 3D-CNN, YOLOv5m, GAN, and BERT methods have minimum F1_{score} of 92.70 %, 95.41 %, 92.37 %, 95.75 %, 93.18 %, 95.03 %, 95.95 %, 92.95 %, and 96.08 %, respectively.

In Table 6 and Fig. 15, the comparative results of the IDLQET-BTEDC model are specified in terms of processing time (PT). The results suggest that the IDLQET-BTEDC method gets better performance. Based on PT, the IDLQET-BTEDC method provides lesser PT of 2.31 sec whereas the Novel 2D-CNN, Novel 3D-CNN, VGG-19, Inception-V3, Fine-tuned VGG-19, and 3D-CNN method attain greater PT values of 6.50 sec, 3.40 sec, 6.83 sec, 7.19 sec, 3.45 sec, 3.78 sec, 5.09 sec, 6.11 sec, and 7.09 sec, correspondingly.

5. Conclusion

In this study, the IDLQET-BTEDC model in MRI images is proposed. The primary goal of the IDLQET-BTEDC model is to improve accuracy and efficiency in identifying BTs using multi-images such as detected and edge images. To accomplish this, the IDLQET-BTEDC approach involves pre-processing, which contains two processes: the wiener filter for noise removal and adaptive gamma correction for contrast enhancement. Next, the segmentation process adopts dual approaches focusing on region and edge detections. The tumour region is segmented using enhanced UNet with NAdam optimization, while the QE edge detection is applied to delineate the tumour boundaries. In addition, the IDLQET-BTEDC model performs feature extraction using Multi-head Attention fusion to combine EfficientNetV2 and ST. The GCRNN classifier is utilized for the BT detection and classification process. Finally, the hyperparameter tuning of the GCRNN model is performed using the STO method to achieve superior accuracy. To demonstrate the good classification outcome of the IDLQET-BTEDC approach, an extensive range of simulations is performed under the Figshare BT dataset. The performance validation of the IDLQET-BTEDC technique portrayed a superior accuracy value of 98.00 % over existing methods. Despite the progress in BT detection and segmentation, current methods still encounter challenges like handling imbalanced datasets, achieving high accuracy across various tumor types, and mitigating model complexity. Many approaches depend on pre-trained NNs, which may not generalize well to various MRI data, resulting in overfitting. Furthermore, noise in MRIs and difficulties in accurate tumor boundary segmentation remain persistent. While some models use TL, hybrid methods, and attention mechanisms, their practical deployment is limited by high computational costs and low interpretability. Future research needs to concentrate on improving robustness, mitigating computational load, and improving generalization in real-world clinical settings.

CRediT authorship contribution statement

Alghamdi Ahmed Mohammed: Writing – original draft, Methodology. **Abdel-Khalek S.:** Writing – review & editing, Writing – original draft, Software. **Alamri Ahmed:** Writing – original draft, Methodology, Investigation. **Bahaddad Adel A.:** Writing – original draft, Validation, Resources.

Declaration of Competing Interest

The authors declare that they have no conflict of interest.

Acknowledgements

This work was funded by the University of Jeddah, Jeddah, Saudi Arabia, under grant No. (UJ-24-DR-1167-1). Therefore, the authors thank the University of Jeddah for its technical and financial support.

Data Availability Statement

The data supporting this study's findings are openly available in the Kaggle repository at <https://www.kaggle.com/datasets/ashkhagan/figshare-brain-tumor-dataset>, reference number [38].

References

- [1] R. Vankothu, M.A. Hameed, Brain tumor MRI image identification and classification based on the recurrent convolutional neural network, *Meas.: Sens.* 24 (2022) 100412.
- [2] Z. Jia, D. Chen, Brain tumor identification and classification of MRI images using deep learning techniques, *IEEE Access* (2020).
- [3] Y. Bhanothu, A. Kamalamannan, G. Rajamanickam, Detection and classification of brain tumors in MRI images using a deep convolutional network. 2020 6th International Conference on Advanced Computing and Communication Systems (ICACCS), IEEE, 2020, March, pp. 248–252.
- [4] J. Amin, M. Sharif, M. Yasmin, S.L. Fernandes, A distinctive approach in brain tumor detection and classification using MRI, *Pattern Recognit. Lett.* 139 (2020) 118–127.
- [5] Kokila, B., Devadharshini, M.S., Anitha, A. and Sankar, S.A., 2021, May. Brain tumor detection and classification using deep learning techniques based on MRI images. In *Journal of Physics: Conference Series* (Vol. 1916, No. 1, p. 012226). IOP Publishing.
- [6] B.T. AL-Nuaimi, R.A. Suhaib, E.S.M. El-kenawy, Adaptive feature selection based on machine learning algorithms for Lung tumors diagnosis and the COVID-19 index, *J. Intell. Syst. Internet Things* 11 (2) (2024).
- [7] A.R. Mathew, P.B. Anto, Tumor detection and classification of MRI brain image using wavelet transform and SVM. 2017 International Conference on signal processing and Communication (ICSPC), IEEE, 2017, July, pp. 75–78.
- [8] C.L. Choudhury, C. Mahanty, R. Kumar, B.K. Mishra, Brain tumor detection and classification using convolutional neural network and deep neural network. 2020 international conference on Computer Science, engineering and Applications (ICCSEA), IEEE, 2020, March, pp. 1–4.
- [9] A. Chaudhary, V. Bhattacharjee, An efficient method for brain tumor detection and categorization using MRI images by K-means clustering & DWT, *Int. J. Inf. Technol.* 12 (1) (2020) 141–148.
- [10] N.N. Mostafa, Human brain tumors detection using neutrosophic c-means clustering algorithm, *J. Neutrosophic Fuzzy Syst.* 1 (2021) 55–55.
- [11] H.A. Vu, S. Vajda, Advancing brain tumor diagnosis: a hybrid approach using edge detection and deep learning. *International Conference on Pattern Recognition*, Springer Nature Switzerland, Cham, 2024, pp. 226–241.
- [12] A.M.G. Allah, A.M. Sarhan, N.M. Elshennawy, Edge U-Net: Brain tumor segmentation using MRI based on deep U-Net model with boundary information, *Expert Syst. Appl.* 213 (2023) 118833.
- [13] Hameed, A., Khan, A., Ahmad, S., Ullah, S., Khan, A.N. and Nawaz, S., 2024. Enhanced Brain Tumor Diagnosis with EfficientNetB6: Leveraging Transfer Learning and Edge Detection Techniques.
- [14] Z. Zhu, X. He, G. Qi, Y. Li, B. Cong, Y. Liu, Brain tumor segmentation is based on the fusion of deep semantics and edge information in multimodal MRI, *Inf. Fusion* 91 (2023) 376–387.
- [15] A.A. Asiri, T.A. Soomro, A.A. Shah, G. Pogrebna, M. Irfan, S. Alqahtani, Optimized brain tumor detection: a dual-module approach for MRI image enhancement and tumor classification, *IEEE Access* 12 (2024) 42868–42887.
- [16] S.C. Prathipati, S.K. Satpathy, A multilevel de-noising approach for precision edge-based fragmentation in MRI brain tumor segmentation, *Traite du Signal* 40 (4) (2023) 1715.
- [17] S. Kanagamalliga, S. Rajappriyaharshine, Brain tumor detection and segmentation using CNN and optimised edge features. 2024 10th International Conference on Communication and Signal Processing (ICCSP), IEEE, 2024, April, pp. 323–327.
- [18] R. Zaitoon, S. Hussain, Enhanced Brain Tumor Detection and Classification in MRI Scans using Convolutional Neural Networks, *Int. J. Adv. Comput. Sci. Appl.* 14 (9) (2023).
- [19] S.P. Rajamohana, V. Yelamali, P. Soni, M. Vanahalli, P. Prasad, Hybrid Quantum Graph Neural Network for Brain Tumor MR Image Classification: HYBRID QUANTUM GRAPH NEURAL NETWORK FOR BRAIN TUMOR MR IMAGE, *J. Sci. Ind. Res. (JSIR)* 84 (1) (2025) 60–71.
- [20] M.S. Ullah, M.A. Khan, A. Masood, O. Mzoughi, O. Saidani, N. Alturki, Brain tumor classification from MRI scans: a framework of hybrid deep learning model with Bayesian optimization and quantum theory-based marine predator algorithm, *Front. Oncol.* 14 (2024) 1335740.
- [21] A. Bilal, M. Shafiq, W.J. Obidallah, Y.A. Alduraywish, H. Long, Quantum computational infusion in extreme learning machines for early multi-cancer detection, *J. Big Data* 12 (1) (2025) 1–48.
- [22] E. Albalawi, A. Thakur, D.R. Dorai, S. Bhatia Khan, T.R. Mahesh, A. Almusharrif, K. Aurangzeb, M.S. Anwar, Enhancing brain tumor classification in MRI scans with a multi-layer customized convolutional neural network approach, *Front. Comput. Neurosci.* 18 (2024) 1418546.
- [23] A. Masood, O. Mzoughi, O. Saidani, hybrid deep learning model with Bayesian optimization and quantum theory-based marine, *Artif. Intell. Imaging Oncol.* (2025) 64.
- [24] M.K. Abd-Ellah, A.I. Awad, A.A. Khalaf, A.M. Ibraheem, Automatic brain-tumor diagnosis using cascaded deep convolutional neural networks with symmetric U-Net and asymmetric residual-blocks, *Sci. Rep.* 14 (1) (2024) 9501.
- [25] S. Katkam, V.P. Tulasi, B. Dhanalaxmi, J. Harikiran, Multi-class Diagnosis of Neurodegenerative Diseases using Effective Deep Learning Models with Modified DenseNet-169 and Enhanced DeepLabV3+, *IEEE Access* (2025).
- [26] M. Aamir, A. Namoun, S. Munir, N. Aljohani, M.H. Alanazi, Y. Alsahafi, F. Alotibi, Brain tumor detection and classification using an optimized convolutional neural network, *Diagnostics* 14 (16) (2024) 1714.
- [27] A. Saeed, K. Shehzad, S.S. Bhatti, S. Ahmed, A.T. Azar, GGLA-NeXtE2NET: A Dual-Branch Ensemble Network with Gated Global-Local Attention for Enhanced Brain Tumor Recognition, *IEEE Access* (2025).
- [28] L. Dénes-Fazakas, L. Kovács, G. Eigner, L. Szilágyi, Enhancing Brain Tumor Diagnosis with L-Net: A Novel Deep Learning Approach for MRI Image Segmentation and Classification, *Biomedicines* 12 (10) (2024) 2388.
- [29] J. Benesty, C. Paleologu, C.L. Stanciu, R.L. Costea, L.M. Dogariu, S. Ciochină, Wiener Filter Using the Conjugate Gradient Method and a Third-Order Tensor Decomposition, *Appl. Sci.* 14 (6) (2024) 2430.
- [30] V.K. Yadav, J. Singhai, Adaptive gamma correction for automatic contrast enhancement of Chest-X-ray images affected by various lung diseases, *Multimed. Tools Appl.* (2024) 1–19.
- [31] Z. Zhou, X. Li, H. Ji, X. Xu, Z. Chang, K. Wu, Y. Song, M. Kao, H. Chen, D. Wu, T. Zhang, Application of improved Unet network in the recognition and segmentation of lung CT images in patients with pneumoconiosis, *BMC Med. Imaging* 24 (1) (2024) 220.
- [32] Q. Aini, Z. Zulfiandi, R. Firmansyah, Y.M. Arif, Applying convolutional neural network and Nadam optimization in flower classification, *Bull. Electr. Eng. Inform.* 13 (4) (2024) 2865–2877.
- [33] S. Abdel-Khalek, G. Abdel-Azim, Z.A. Abo-Eleneen, A.S.F. Obada, New approach to image edge detection based on quantum entropy, *J. Russ. Laser Res.* 37 (2016) 141–154.
- [34] Y. Sun, L. Ning, B. Zhao, J. Yan, Tomato Leaf Disease Classification by Combining EfficientNetv2 and a Swin Transformer, *Appl. Sci.* 14 (17) (2024) 7472.
- [35] Y. Song, L. Liu, Y. Rao, X. Zhang, X. Jin, FA-Net: a fused feature for multi-head attention recoding network for pear leaf nutritional deficiency diagnosis with visual RGB-image depth and shallow features, *Sensors* 23 (9) (2023) 4507.
- [36] A. Zanfei, B.M. Brentan, A. Menapace, M. Righetti, M. Herrera, Graph convolutional recurrent neural networks for water demand forecasting, *Water Resour. Res.* 58 (7) (2022) e2022WR032299.
- [37] N. Eini, S. Janizadeh, S.M. Bateni, C. Jun, E. Heggy, M. Kirs, Predicting equilibrium scour depth around non-circular bridge piers with shallow foundations using hybrid explainable machine learning methods, *Results Eng.* (2024) 103492.
- [38] (<https://www.kaggle.com/datasets/ashkhagan/figshare-brain-tumor-dataset>).
- [39] W. Alghamdi, Computer-aided aided brain tumor diagnosis using coati optimization algorithm with explainable artificial intelligence approach, *Fusion.: Pract. Appl.* (2) (2025) 24–24.
- [40] S. Stephe, V. Nivedita, B. Karthikeyan, K. Nithya, M.Y. Sikkandar, Enhancing brain tumor detection and classification using osprey optimization algorithm with deep learning on MRI images, *J. Intell. Syst. Internet Things* 12 (1) (2024).
- [41] T. Vaiyapuri, J. Mahalingam, S. Ahmad, H.A. Abdeljaber, E. Yang, S.Y. Jeong, Ensemble learning-driven computer-aided diagnosis model for brain tumor classification on magnetic resonance imaging, *IEEE Access* 11 (2023) 91398–91406.
- [42] F. Ullah, M. Nadeem, M. Abrar, M. Al-Razgan, T. Alfakih, F. Amin, A. Salam, Brain tumor segmentation from MRI images using handcrafted convolutional neural network, *Diagnostics* 13 (16) (2023) 2650.
- [43] H. Alquran, M. Alslatie, A. Rababah, W.A. Mustafa, Improved brain tumor segmentation in MR images with a modified U-Net, *Appl. Sci.* 14 (15) (2024) 6504.
- [44] M. Zhou, M.W. Wagner, U. Tabori, C. Hawkins, B.B. Ertl-Wagner, F. Khalvati, Generating 3D brain tumor regions in MRI using vector-quantization Generative Adversarial Networks, *Comput. Biol. Med.* 185 (2025) 109502.
- [45] S. Muksimova, S. Umirkazova, S. Mardieva, N. Iskhakova, M. Sultanov, Y.I. Cho, A lightweight attention-driven YOLOv5m model for improved brain tumor detection, *Comput. Biol. Med.* 188 (2025) 109893, <https://doi.org/10.1016/j.combiomed.2025.109893>.